optica

Deep-subwavelength plasmonic mode converter with large size reduction for Si-wire waveguide

Masaaki Ono,[1,2,4] Hideaki Taniyama,[1,2] Hao Xu,[1,2] Masato Tsunekawa,[2,3] Eiichi Kuramochi,[1,2] Kengo Nozaki,[1,2] and Masaya Notomi[1,2,3,5]

[1]Nanophotonics Center, NTT Corporation, 3-1, Morinosato Wakamiya, Atsugi, Kanagawa 243-0198, Japan
[2]NTT Basic Research Laboratories, NTT Corporation, 3-1, Morinosato Wakamiya, Atsugi, Kanagawa 243-0198, Japan
[3]Department of Physics, Tokyo Institute of Technology, 2-12-1, Ookayama, Meguro-ku, Tokyo 152-8550, Japan
[4]e-mail: ono.masaaki@lab.ntt.co.jp
[5]e-mail: notomi.masaya@lab.ntt.co.jp

Received 1 June 2016; revised 2 August 2016; accepted 9 August 2016 (Doc. ID 267062); published 2 September 2016

If we are to utilize deep-subwavelength plasmonic waveguides in photonic integrated circuit applications, highly efficient three-dimensional (3D) mode conversion must be achieved between deep-subwavelength plasmonic waveguides and conventional dielectric waveguides such as Si-wire waveguides. Here, we describe 3D mode conversion from a Si-wire waveguide (the core size is 400 nm × 200 nm) to a plasmonic slot waveguide (the air core size is 50 nm × 20 nm) with a coupling loss of 1.7 dB. Our mode converter has only a two-dimensional laterally tapered structure even with the presence of a large discontinuity in the thickness, and can still produce efficient full 3D mode conversion with a very short taper length (600 nm). Calculation results obtained with the finite element method agreed well with the experimental results. We believe our mode converter will provide a new deep-subwavelength photonic platform.

OCIS codes: (220.4241) Nanostructure fabrication; (240.6680) Surface plasmons; (250.5300) Photonic integrated circuits; (250.5403) Plasmonics; (310.6628) Subwavelength structures, nanostructures.

http://dx.doi.org/10.1364/OPTICA.3.000999

1. INTRODUCTION

It is well recognized that light-propagating modes in plasmonic waveguides can be squeezed beyond the diffraction limit [1]. Because of their potential for use in constructing ultracompact photonic devices and for greatly enhancing light–matter interactions, plasmonic waveguides are expected to play a crucial role in photonic integrated circuit applications. Recently, various types of optical devices based on plasmonic waveguides have been demonstrated, including detectors [2,3], modulators [4,5], and light sources [6–8]. As regards plasmonic waveguides, a metal–insulator–metal (MIM) waveguide, which is a plasmonic analog of radiofrequency two-conductor electric lines, is known to have an extremely small effective mode cross-section [9]. Lateral MIM waveguides can be fabricated with conventional nanofabrication processes, and deep-subwavelength MIM waveguides with an approximately 50 nm × 50 nm cross-section have been already reported [10,11].

Although plasmonic waveguides are generally superior in terms of mode size, this is usually accompanied by a large propagation loss [9], which may suppress the expected advantages. It is thus natural to consider combining plasmonic waveguides with conventional low-loss dielectric waveguides to construct a full circuit. If each plasmonic device is shorter than 10 μm and longer distance connection is achieved with dielectric waveguides, the propagation loss may not be a serious issue. This means that an efficient mode converter between plasmonic and dielectric modes is of significant importance. However, it is generally difficult to connect two waveguide modes that have fundamentally different sizes and characteristics. Hence, this type of converter is now considered to be one of the most critically important components for various plasmonics applications.

Recently, several types of mode converters for use between a Si-wire dielectric waveguide and a lateral MIM waveguide have been proposed and demonstrated [4,12–18]. Although a fairly high conversion efficiency has been reported, the vertical thickness of the MIM waveguides was about the same as that of Si-wire waveguides (around 200 nm), which loses the advantage of the ultimate smallness of MIM waveguides (the thickness can be as little as 10–20 nm). This means that they are essentially two-dimensional (2D) mode converters, where the mode size is squeezed only laterally through the use of a laterally tapered structure. The cross-sectional core size of MIM waveguides used in these converters is mostly around $(\lambda/n)^2/100$ or larger (λ = wavelength, n = refractive index of the waveguide core) [4,12–18], although it is not difficult to realize deep-subwavelength MIM waveguides with a dimension smaller than $(\lambda/n)^2/1000$ [11]. In addition, the most efficient mode converters are generally long (>1 μm), which also makes it difficult to

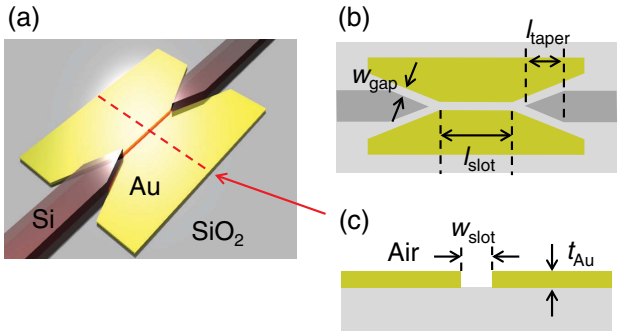

Fig. 1. (a) Schematic structure of the mode converter. The width and height of the Si-wire waveguide are 400 and 200 nm, respectively. (b) Cross-sectional top view of the structure. (c) Cross-sectional side view of the MIM waveguide at the red broken line shown in (a).

realize compact plasmonic components. It is clear that a full three-dimensional (3D) mode converter, where the mode size is squeezed laterally and vertically, is better; however, we then have to overcome an abrupt change in the vertical thickness, which may greatly reduce the conversion efficiency. A full 3D (laterally and vertically) tapered structure has been employed in a nanofocusing component, but the structure and fabrication process are rather complicated [19,20]. Consequently, the key issues are to realize a compact mode converter for connecting a Si-wire dielectric waveguide to a deep-subwavelength MIM waveguide when there is a large mismatch in the vertical thickness, and to achieve efficient 3D mode conversion without introducing a complicated fabrication process.

In this study, we propose and demonstrate a simple and highly efficient mode converter between a Si-wire waveguide [400 nm × 200 nm, corresponding to $(\lambda/n)^2/2.5$] and a deep-subwavelength lateral MIM waveguide consisting of gold and air, known as a plasmonic slot waveguide [the air core size is 50 nm × 20 nm, corresponding to $(\lambda/n)^2/2000$]. A key feature is that our converter [shown in Fig. 1(a)] has only a 2D laterally tapered structure even with the presence of a large discontinuity in the thickness, yet can still produce efficient, full 3D mode conversion with a very short taper length. We first present our theoretical design and clarify how we can achieve high conversion efficiency with a simple 2D taper. Then, after showing the fabrication procedure, we present our experimental demonstration of plasmonic mode converters with a series of different parameters. These experiments reveal that our plasmonic mode converters exhibit very high conversion efficiency with a very small taper length, even when there is a large mismatch in vertical thickness.

2. DESIGN OF MODE CONVERTER

We numerically investigate the structure shown in Figs. 1(a)–1(c) using the finite element method (FEM) and assuming a transverse electric (TE) polarized input. Here, we assume an ultra-thin MIM waveguide (vertical thickness, 20 nm) connected to a conventional Si-wire waveguide (vertical thickness, 200 nm). We took the permittivities of Au, Si, and SiO_2 from previous studies [21,22]. Figure 2(a) is a top view of the calculated field profile ($|E_x|^2$) of the structure with a taper length l_{taper} of 400 nm and a 50 nm × 20 nm slot at a wavelength of 1550 nm. We assumed a gap $w_{gap} = 40$ nm between the Si taper and metal, which we will later show to be critical as regards improving the coupling efficiency. Figure 2(b) shows cross-sectional mode profiles in the Si-wire waveguide, the mode conversion part, and the MIM waveguide. Within the tapered region, the mode profile gradually changes from the profile of the eigenmode of the Si-wire waveguide to that of the MIM waveguide (left to right). Note that the eigenmode of the Si-wire waveguide has two side lobes outside the Si core, which has a somewhat similar mode profile to that in the MIM waveguide. When the optical field propagates from the Si waveguide to the tapered part, these side lobes gradually increase in size as a result of the interaction with the surrounding metal placed in the vicinity of the Si waveguide, and they are finally adiabatically coupled to the eigenmode of the MIM waveguide. Here, we observe that the guiding mode is

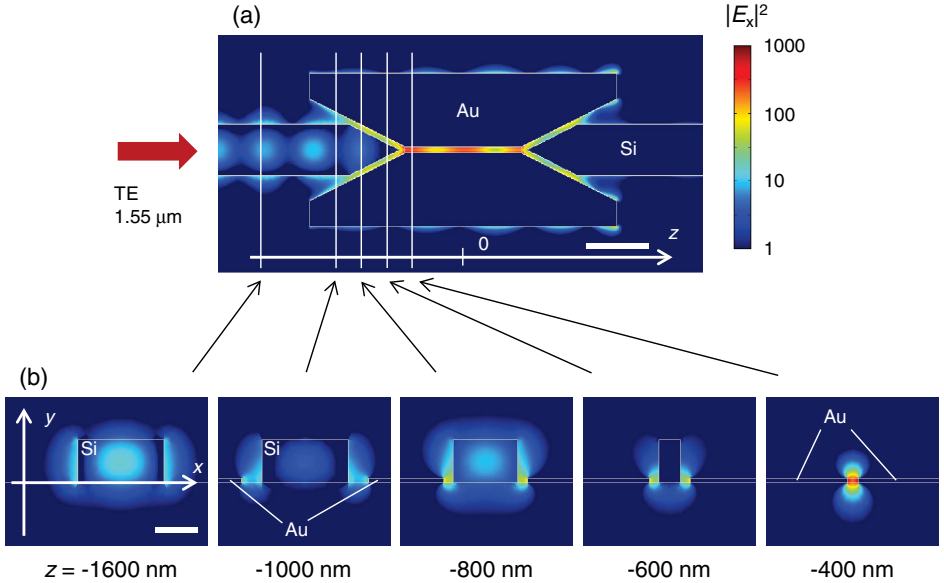

Fig. 2. (a) Cross-sectional top view of the calculated field profile at $y = 10$ nm. Scale bar, 500 nm. (b) Cross-sectional side views of the calculated field profile in the tapered region. Scale bar, 200 nm.

successfully converted from the Si-wire waveguide to the MIM waveguide. The existence of the side lobes makes it possible to realize a high coupling efficiency even when there is a large thickness mismatch. In addition, the air gap between the Si and the metal introduces the side lobes into the MIM waveguide efficiently and reduces the absorption loss in the mode conversion. As shown subsequently, the presence of the air gap further improves the coupling efficiency.

Next, we quantitatively evaluated the optical loss of our structure. First, we estimated the total loss of the whole structure by calculating the transmittance via input/output waveguides. The propagation loss was then deduced from the effective index (n_{eff}) of the eigenmode in MIM waveguides (see Supplement 1). The calculated propagation loss for an Au thickness t_{Au} of 20 nm and a slot width w_{slot} of 50 nm was 1.3 dB/μm. The coupling loss was estimated from the total loss minus the propagation loss. Thus, the coupling loss includes the metal absorption in the tapered region and the reflection and scattering (see Supplement 1). For a typical sample (a 50 nm × 20 nm slot with a slot length $l_{\mathrm{slot}} = 0.92$ μm, $l_{\mathrm{taper}} = 400$ nm, and $w_{\mathrm{gap}} = 40$ nm), the total loss, propagation loss, and coupling loss per converter were 8.2 dB, 1.3 dB/μm, and 3.5 dB, respectively. This coupling efficiency (−3.5 dB) is already high and is comparable to that of previously reported 2D mode converters for much thicker MIM waveguides [12–14].

Furthermore, we investigated the structural parameter dependence of the coupling efficiency to allow us to optimize the converters. Figure 3(a) shows the l_{taper} dependence of the coupling loss for $t_{\mathrm{Au}} = 20$ nm and $w_{\mathrm{gap}} = 40$ nm. The coupling loss decreases when l_{taper} becomes longer, as expected. We confirmed that the loss decreases monotonically until $l_{\mathrm{taper}} = 600$ nm. However, a more important finding is that we can achieve a fairly high efficiency even for a taper much shorter than 1 μm. The estimated coupling loss is around 1.4 dB at $l_{\mathrm{taper}} = 600$ nm. We also varied w_{slot} between 50 and 70 nm and found that the coupling loss is almost independent of w_{slot}, indicating that a smaller w_{slot} will be better in terms of obtaining a large field enhancement. When we varied t_{Au} [Fig. 3(b)], the coupling loss decreased as t_{Au} increased. However, it should be noted that the rate at which the coupling loss changed with respect to t_{Au} was much smaller than that of t_{Au} around $l_{\mathrm{taper}} = 600$ nm, which means that the field enhancement would be even larger for a smaller t_{Au}. This dependence on w_{slot} and t_{Au} is important because it is generally not easy to achieve a high coupling efficiency and strong field confinement simultaneously. Our result shows that a smaller w_{slot} and a smaller t_{Au} would be better at least within the parameter range we simulated. Note that when $t_{\mathrm{Au}} = 20$ nm and $w_{\mathrm{slot}} = 50$ nm (in fact, they are the smallest t_{Au} and w_{slot} we fabricated), the coupling loss of our mode converter reached 1.4 dB at $l_{\mathrm{taper}} = 600$ nm.

Next, we investigated the w_{gap} dependence of the coupling efficiency. Figure 3(c) shows the w_{gap} dependence of the coupling loss for a fixed l_{taper} of 600 nm and a 50 nm × 20 nm slot. Note that the coupling loss is very high without the gap. When there is a small air gap, the coupling loss is clearly reduced and reaches its minimum value at around $w_{\mathrm{gap}} = 20$ nm. The minimum coupling loss is as small as 0.95 dB at $w_{\mathrm{gap}} = 20$ nm. As w_{gap} is further increased, the coupling loss increases again. At $w_{\mathrm{gap}} = 100$ nm, efficient mode conversion is no longer achieved. As mentioned previously, the eigenmode of the Si-wire waveguide has side lobes, which should be adiabatically connected to the MIM mode for efficient conversion. These side lobes are mainly absorbed or scattered when $w_{\mathrm{gap}} = 0$ nm, and most of the side lobes are scattered when $w_{\mathrm{gap}} = 100$ nm (see Supplement 1). This leads to poor conversion efficiency at $w_{\mathrm{gap}} = 0, 100$ nm. Thus, the gap plays an important role in mode conversion.

The calculated results showed that we can achieve highly efficient 3D mode conversion from a thick Si-wire waveguide to a very thin MIM waveguide butt-jointed with a simple 2D taper. When we choose the optimum structural parameters, our mode converter with a fairly short taper length of 600 nm can achieve a coupling loss of 0.95 dB between a Si-wire waveguide with a cross-section of 400 nm × 200 nm [corresponding to $(\lambda/n)^2/2.5$] and a deep-subwavelength MIM waveguide with a cross-section of 50 nm × 20 nm [corresponding to $(\lambda/n)^2/2000$]. The predicted performance is excellent in terms of the size reduction of the waveguide core, coupling efficiency, and taper length in comparison to previous mode converters. A detailed comparison is provided later.

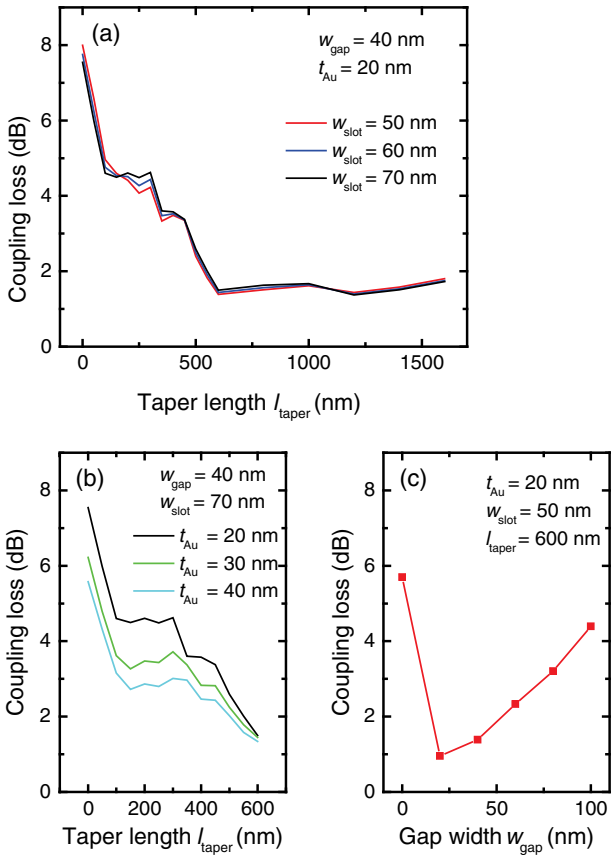

Fig. 3. Calculated coupling loss. Taper length dependence of the coupling loss for (a) Au thickness of 20 nm and slot widths of 50–70 nm and (b) Au thicknesses of 20–40 nm and slot width of 70 nm. (c) Gap width dependence of the calculated coupling loss for a taper length of 600 nm.

3. FABRICATION

We first prepared Si-wire waveguides (400 nm × 200 nm) on a silicon-on-insulator substrate with electron beam (EB) lithography (an acceleration voltage of 100 kV) and an etching process. We then formed Au MIM waveguides using EB lithography, evaporation (an Au layer was evaporated after a 1 nm Ti layer), and a liftoff process. Using this approach, we fabricated mode

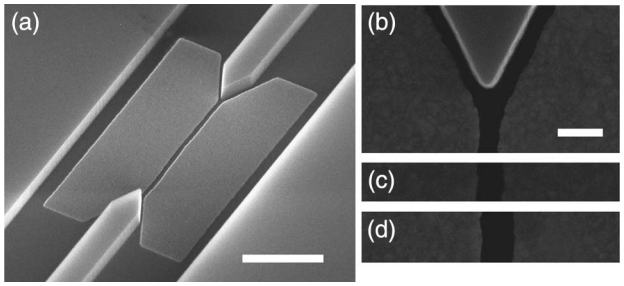

Fig. 4. (a) SEM image of the fabricated mode converter with a taper length of 400 nm, 70 nm × 20 nm slot, and 40 nm gap between the Si taper and metal. Scale bar, 1 μm. (b)–(d) Top-view SEM images for slot widths of (b) 50, (c) 60, and (d) 70 nm. Scale bar, 100 nm.

converters with a series of different parameters (t_{Au} = 20, 30, 40 nm; w_{slot} = 50, 60, 70 nm; l_{taper} = 0–600 nm; w_{gap} = 40–90 nm). Figure 4(a) is a scanning electron microscopy (SEM) image of the fabricated mode converter. Figures 4(b)–4(d) are magnified images of the region around the slot and taper edge, showing that they were successfully fabricated with precise positioning. Misalignments between Si-wire waveguides and MIM waveguides were smaller than 20 nm. To achieve this high position accuracy, we used a fine pitch alignment mark (2.5 mm × 2.8 mm). As explained previously, we used only conventional nanofabrication processes in this fabrication procedure, which is compatible with conventional plasmonics, photonic crystals, and Si photonics devices. This compatibility is one of the important merits and will enable us to utilize the mode converters with other photonic structures in photonic integrated circuits.

4. RESULTS AND DISCUSSION

The solid blue line in Fig. 5(a) shows the optical transmission spectrum of fabricated sample A (50 nm × 20 nm slot, l_{slot} = 0.92 μm, l_{taper} = 400 nm, w_{gap} = 40 nm). We input continuous-wave wavelength-tunable laser light in the TE mode and measured the output power intensity. The data include fine Fabry–Perot (FP) oscillation, and are fitted with a third-order polynomial to investigate the intrinsic transmittance without the FP oscillations. This fitted line was almost independent of the wavelength within the measured wavelength range. Compared to the transmittance of a reference Si-wire waveguide [reference, shown in Fig. 5(a)], the average relative transmittance (T) in the measured wavelength range was −7.5 dB. This value is close to the transmittance obtained with the FEM as shown previously (−8.2 dB). We also prepared two other reference samples [B and C, shown in Fig. 5(a)]. Sample B had no metal parts between the two tapered Si-wire waveguides, and sample C had no slot in the metal. The T of sample B was −19 dB, and that of sample C was even smaller (< − 20 dB). These two reference results clearly exclude the possibility that the high transmittance of our mode converter is due to light propagation outside the slot.

The coupling and propagation losses were obtained by the linear fitting of the measured l_{slot} dependence of T shown in Fig. 5 (b). The estimated coupling and propagation losses were 3.3 dB and 1.8 dB/μm, respectively, for the 50 nm × 20 nm slot, l_{taper} = 400 nm, and w_{gap} = 40 nm. These values are also consistent with the calculation results obtained with the FEM

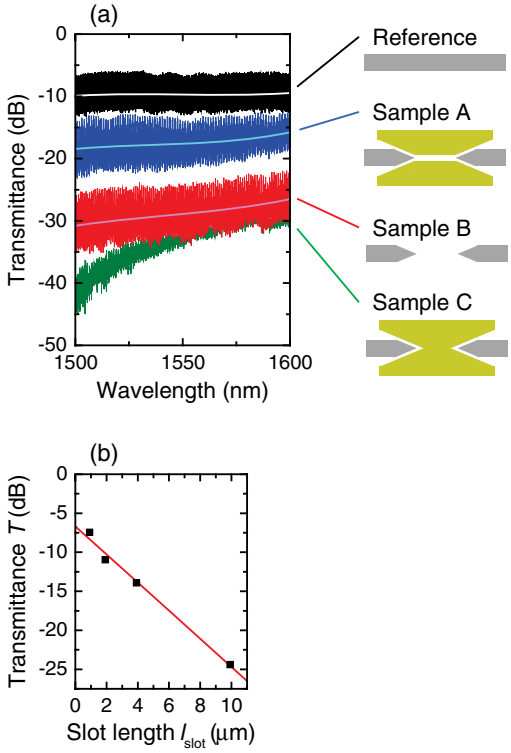

Fig. 5. (a) Transmission spectra of the mode converter (sample A) and reference structures (reference, reference Si-wire waveguide; sample B, structure without metal parts; sample C, structure without a slot in the metal). The Fabry–Perot (FP) oscillation is caused by large reflectance at the cleaved sample edges and finite reflectance at the central element. This FP oscillation is consistent with the reflectance estimated in Fig. S2 (see Supplement 1). (b) Slot length dependence of the transmittance T, which is the average relative transmittance in the measured wavelength range, in sample A.

(the calculated coupling and propagation losses were 3.5 dB and 1.3 dB/μm, respectively).

Next, we investigated the transmittance characteristics of a series of samples with different structural parameters (l_{taper}, w_{slot}, t_{Au}, w_{gap}). First, we investigated the l_{taper} dependence of the coupling loss [solid red line in Fig. 6(a)] for w_{slot} = 50 nm, t_{Au} = 20 nm, and w_{gap} = 40 nm, which corresponds to the smallest cross-section we fabricated. The coupling loss decreased as l_{taper} became longer, and achieved a significantly small value of 1.7 dB at l_{taper} = 600 nm. Note that this loss value is rather close to the calculated loss (1.4 dB), and the l_{taper} dependence shown in this figure agrees very well with the calculation results [solid red line in Fig. 3(a)]. The w_{slot} and t_{Au} dependence of the coupling loss is also shown in Figs. 6(a) and 6(b). Figure 6(a) shows that the coupling loss exhibits very little w_{slot} dependence (from 50 to 70 nm). In terms of t_{Au}, Fig. 6(b) shows that the coupling loss decreases slightly, as t_{Au} is increased from 20 to 40 nm. When l_{taper} = 600 nm, the coupling loss is 1.2–1.3 dB for all t_{Au}, which is the smallest value we measured. When l_{taper} becomes shorter than 600 nm, the loss begins to depend slightly on t_{Au}, as shown in Fig. 6(b). Note that the coupling loss is less than 3 dB at l_{taper} = 200 nm when t_{Au} = 30 and 40 nm, and the loss is still around 4 dB even at l_{taper} = 0 nm when t_{Au} = 40 nm. The overall results in Figs. 6(a) and 6(b) agree surprisingly well over various

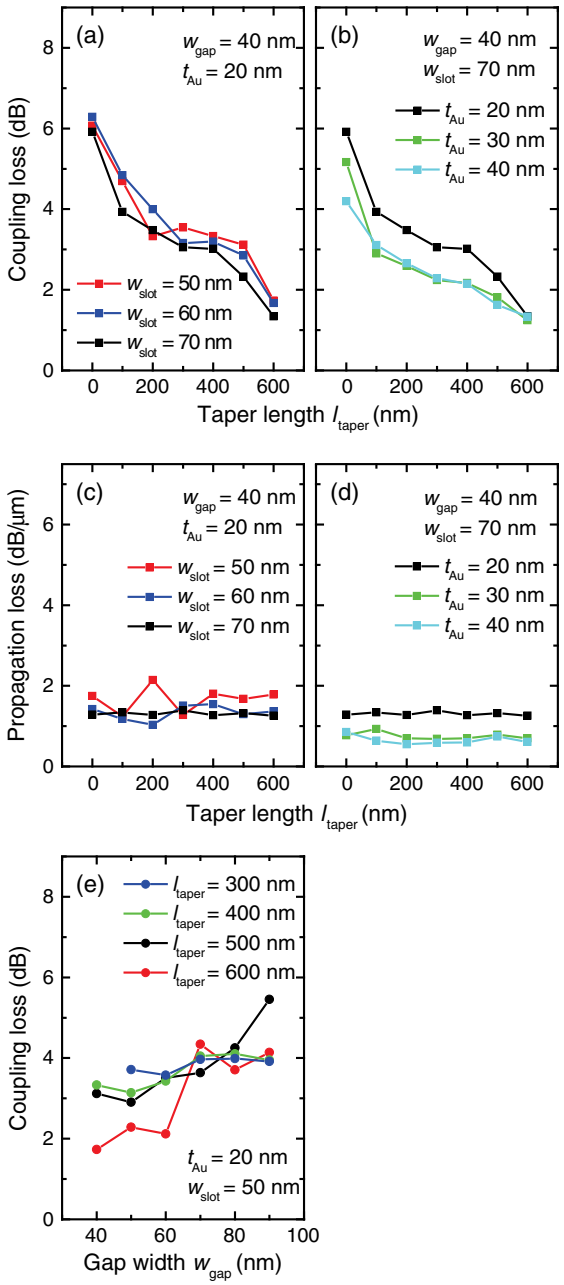

Fig. 6. Coupling and propagation losses obtained with a transmission measurement. Taper length dependence of the coupling loss for (a) Au thickness of 20 nm and slot widths of 50–70 nm and (b) Au thicknesses of 20–40 nm and slot width of 70 nm. Taper length dependence of the propagation loss for (c) Au thickness of 20 nm and slot widths of 50–70 nm and (d) Au thicknesses of 20–40 nm and slot width of 70 nm. (e) Gap width dependence of the coupling loss for taper lengths of 300–600 nm.

parameters with the corresponding calculated results shown in Figs. 3(a) and 3(b). This agreement clearly proves that the theoretically predicted high performance is indeed realized in the present plasmonic mode converters, and also guarantees the robustness of our design.

The measured propagation loss data are shown as a function of l_{taper} in Figs. 6(c) and 6(d) for different w_{slot} and t_{Au} values. The propagation loss does not exhibit any noticeable dependence on l_{taper}, which is as expected and proves the accuracy of our estimation. The loss decreases slightly as t_{Au} increases, and the dependence on w_{slot} is very small. These characteristics of the propagation loss as a function of w_{slot} and t_{Au} are consistent with our calculation (see Supplement 1), and the resultant loss values (for example, 1.8 dB/μm for $w_{slot} = 50$ nm and $t_{Au} = 20$ nm) are fairly close to the predicted theoretical propagation loss (1.3 dB/μm). The agreement with the theory demonstrates the credibility of our fabrication method.

As discussed in the design section, the coupling efficiency depends on w_{gap}. Figure 6(e) shows the w_{gap} dependence of the coupling loss for samples fabricated with $l_{taper} = 300$–600 nm and a 50 nm × 20 nm slot. The coupling loss increased as w_{gap} became larger for all the l_{taper} values that we investigated here. This dependence is consistent with the calculation results [Fig. 3(c)]. As described before in the design section, the coupling loss can be further reduced below 1 dB, at least theoretically, if we can reduce w_{gap}. Thus, it is still important to improve the fabrication resolution if we wish to achieve much finer structures.

Finally, we compared our result with previous demonstrations of plasmonic mode converters for Si-wire waveguides (the cross-section is typically around 400 nm × 200 nm for telecom wavelengths) and lateral MIM waveguides [4,12–18]. In the experiment just described, we demonstrated highly efficient 3D mode conversion from a Si-wire waveguide to a deep-subwavelength MIM waveguide, and showed that l_{taper} and w_{gap} are important for efficient 3D mode conversion. The obtained coupling and propagation losses were 1.7 dB and 1.8 dB/μm, respectively, for the 50 nm × 20 nm slot, $l_{taper} = 600$ nm, and $w_{gap} = 40$ nm. In terms of the MIM waveguide core size, $(\lambda/n)^2/120$ was achieved by Salamin *et al.* [5,18], which is the lowest reported value to the best of our knowledge. The core size of our MIM waveguide is $(\lambda/n)^2/2000$, which is 14 times smaller and lies deep in the subwavelength regime. The core size reduction ratio in relation to the input Si-wire waveguide is as large as 800, which is also much larger than previously reported values. An important fact is that we achieved this large core size reduction simultaneously with a high coupling efficiency (−1.7 dB) and short taper length (600 nm). In fact, this coupling efficiency is the highest value and the taper length is the shortest value among similar plasmonic mode converters for Si-wire waveguides [4,12–15,17,18] except for structures whose MIM waveguide cores are silicon [16], where the MIM waveguide core sizes are much larger than ours. This clearly shows the significant advantages of our converter design, which overcame the large vertical thickness mismatch.

Such a high coupling efficiency and large core size reduction ratio should lead to a large enhancement of the optical field in the MIM waveguide. Here, we evaluate the field intensity enhancement in the fabricated plasmonic mode converters by numerically estimating the field enhancement factor η defined as $\eta = (\int_{slot} |E|^2 dS / \int_{slot} dS)/(\int_{Si\text{-}wire} |E|^2 dS / \int_{Si\text{-}wire} dS)$ with the FEM calculation. η stands for the ratio of the field intensity averaged over the cross-section of each waveguide core (see Supplement 1). In Fig. 7, we plot η estimated at the entrance of the MIM waveguide, which includes the coupling loss, for $l_{taper} = 600$ nm and various w_{slot} and t_{Au} values. η increases as w_{slot} becomes smaller or t_{Au} becomes thinner. The maximum η for the fabricated samples is 41 when $w_{slot} = 50$ nm and $t_{Au} = 20$ nm. This is a very large value when we consider the

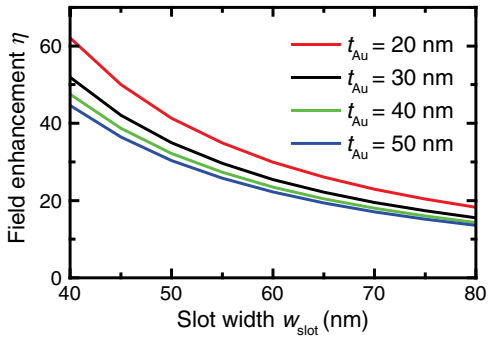

Fig. 7. Field enhancement factor η, which is the ratio of the electric field intensity averaged over a cross-section of the MIM waveguide slot to that of the Si-wire waveguide core, at the entrance of the MIM waveguide for a taper length of 600 nm.

fact that the light field is already squeezed in the input high-index Si-wire waveguide. Although a larger enhancement ratio was reported for plasmonic nano-focusing elements without dielectric waveguides [11,20], the η value for our converter is the largest among plasmonic mode converters for Si-wire waveguides to the best of our knowledge. We also estimated the effective cross-sectional area [23], which is another quantity related to the enhancement. The estimated value for $w_{slot} = 50$ nm and $t_{Au} = 20$ nm is as small as 6×10^{-4} μm^2. Obviously, η at the mid-point in the slot will be slightly reduced due to the finite propagation loss of the MIM waveguide, but this reduction can be kept small if the slot length is sufficiently short.

5. CONCLUSIONS

We have demonstrated highly efficient 3D mode conversion from a Si-wire waveguide (400 nm × 200 nm) to a deep-subwavelength MIM (plasmonic slot) waveguide (50 nm × 20 nm) without using a complicated 3D tapered structure. Our calculation revealed that w_{gap} and l_{taper} are important for efficient 3D mode conversion and predicted that the theoretical coupling loss of the mode converter with optimum structural parameters is 1.4 dB when $l_{taper} = 600$ nm and $w_{gap} = 40$ nm, and can be further reduced to 0.95 dB when $w_{gap} = 20$ nm. In accordance with this design, we fabricated plasmonic mode converters with a series of different parameters. With the transmission measurements, we confirmed a coupling loss of 1.7 dB when $l_{taper} = 600$ nm and $w_{gap} = 40$ nm. The core size of the connected MIM waveguide is $(\lambda/n)^2/2000$, which is the smallest value, and the achieved size reduction ratio, 800, is the largest among previous plasmonic converters. In spite of the large size reduction, our mode converters can function with a very high coupling efficiency and an ultrashort length, which are the best values for low-index core MIM waveguides. The estimated field intensity enhancement factor η was 41. In addition, it is worth noting that the measured results agree very well with numerically simulated results over a wide range of parameters. Considering the fact that the core size of plasmonic mode converters is deep in the subwavelength regime, this agreement is convincing as regards the robustness of our design.

The highly efficient ultracompact 3D mode conversion that we have achieved will enable us to utilize deep-subwavelength plasmonic waveguides with large field enhancement in various applications. We believe that our mode converter will provide a new deep-subwavelength photonic platform. Moreover, the size of the waveguide slot almost matched the dimensions of such nanomaterials as quantum dots or nanowires, and therefore will greatly increase the light–matter interaction cross-section with nanomaterials. Hence, appropriate combinations with functional materials may lead to ultralow-power photonic devices for photonic integrated circuits and single-photon devices for quantum information processing [24,25].

Funding. Japan Society for the Promotion of Science (JSPS) KAKENHI (JP15H05735).

Acknowledgment. We thank T. Tamamura for support with the fabrication and H. Onji for support with the measurement.

See Supplement 1 for supporting content.

REFERENCES

1. D. K. Gramotnev and S. I. Bozhevolnyi, "Plasmonics beyond the diffraction limit," Nat. Photonics **4**, 83–91 (2010).
2. Z. Han, I. P. Radko, N. Mazurski, B. Desiatov, J. Beermann, O. Albrektsen, U. Levy, and S. I. Bozhevolnyi, "On-chip detection of radiation guided by dielectric-loaded plasmonic waveguides," Nano Lett. **15**, 476–480 (2015).
3. P. Neutens, P. Van Dorpe, I. De Vlaminck, L. Lagae, and G. Borghs, "Electrical detection of confined gap plasmons in metal–insulator–metal waveguides," Nat. Photonics **3**, 283–286 (2009).
4. A. Melikyan, L. Alloatti, A. Muslija, D. Hillerkuss, P. C. Schindler, J. Li, R. Palmer, D. Korn, S. Muehlbrandt, D. Van Thourhout, B. Chen, R. Dinu, M. Sommer, C. Koos, M. Kohl, W. Freude, and J. Leuthold, "High-speed plasmonic phase modulators," Nat. Photonics **8**, 229–233 (2014).
5. C. Haffner, W. Heni, Y. Fedoryshyn, J. Niegemann, A. Melikyan, D. L. Elder, B. Baeuerle, Y. Salamin, A. Josten, U. Koch, C. Hoessbacher, F. Ducry, L. Juchli, A. Emboras, D. Hillerkuss, M. Kohl, L. R. Dalton, C. Hafner, and J. Leuthold, "All-plasmonic Mach–Zehnder modulator enabling optical high-speed communication at the microscale," Nat. Photonics **9**, 525–528 (2015).
6. K. C. Y. Huang, M. K. Seo, T. Sarmiento, Y. J. Huo, J. S. Harris, and M. L. Brongersma, "Electrically driven subwavelength optical nanocircuits," Nat. Photonics **8**, 244–249 (2014).
7. P. Neutens, L. Lagae, G. Borghs, and P. Van Dorpe, "Electrical excitation of confined surface plasmon polaritons in metallic slot waveguides," Nano Lett. **10**, 1429–1432 (2010).
8. Y. S. No, J. H. Choi, H. S. Ee, M. S. Hwang, K. Y. Jeong, E. K. Lee, M. K. Seo, S. H. Kwon, and H. G. Park, "A double-strip plasmonic waveguide coupled to an electrically driven nanowire LED," Nano Lett. **13**, 772–776 (2013).
9. G. Veronis and S. H. Fan, "Modes of subwavelength plasmonic slot waveguides," J. Lightwave Technol. **25**, 2511–2521 (2007).
10. M. Schnell, P. Alonso-González, L. Arzubiaga, F. Casanova, L. E. Hueso, A. Chuvilin, and R. Hillenbrand, "Nanofocusing of mid-infrared energy with tapered transmission lines," Nat. Photonics **5**, 283–287 (2011).
11. M. P. Nielsen, L. Lafone, A. Rakovich, T. P. Sidiropoulos, M. Rahmani, S. A. Maier, and R. F. Oulton, "Adiabatic nanofocusing in hybrid gap plasmon waveguides on the silicon-on-insulator platform," Nano Lett. **16**, 1410–1414 (2016).
12. L. Chen, J. Shakya, and M. Lipson, "Subwavelength confinement in an integrated metal slot waveguide on silicon," Opt. Lett. **31**, 2133–2135 (2006).
13. J. Tian, S. Yu, W. Yan, and M. Qiu, "Broadband high-efficiency surface-plasmon-polariton coupler with silicon-metal interface," Appl. Phys. Lett. **95**, 013504 (2009).

14. Z. Han, A. Y. Elezzabi, and V. Van, "Experimental realization of subwavelength plasmonic slot waveguides on a silicon platform," Opt. Lett. **35**, 502–504 (2010).
15. R. X. Yang, R. A. Wahsheh, Z. L. Lu, and M. A. G. Abushagur, "Efficient light coupling between dielectric slot waveguide and plasmonic slot waveguide," Opt. Lett. **35**, 649–651 (2010).
16. S. Zhu, T. Y. Liow, G. Q. Lo, and D. L. Kwong, "Silicon-based horizontal nanoplasmonic slot waveguides for on-chip integration," Opt. Express **19**, 8888–8902 (2011).
17. A. Melikyan, K. Koehnle, M. Lauermann, R. Palmer, S. Koeber, S. Muehlbrandt, P. C. Schindler, D. L. Elder, S. Wolf, W. Heni, C. Haffner, Y. Fedoryshyn, D. Hillerkuss, M. Sommer, L. R. Dalton, D. Van Thourhout, W. Freude, M. Kohl, J. Leuthold, and C. Koos, "Plasmonic-organic hybrid (POH) modulators for OOK and BPSK signaling at 40 Gbit/s," Opt. Express **23**, 9938–9946 (2015).
18. Y. Salamin, W. Heni, C. Haffner, Y. Fedoryshyn, C. Hoessbacher, R. Bonjour, M. Zahner, D. Hillerkuss, P. Leuchtmann, D. L. Elder, L. R. Dalton, C. Hafner, and J. Leuthold, "Direct conversion of free space millimeter waves to optical domain by plasmonic modulator antenna," Nano Lett. **15**, 8342–8346 (2015).
19. S. Vedantam, H. Lee, J. Tang, J. Conway, M. Staffaroni, and E. Yablonovitch, "A plasmonic dimple lens for nanoscale focusing of light," Nano Lett. **9**, 3447–3452 (2009).
20. H. Choo, M. K. Kim, M. Staffaroni, T. J. Seok, J. Bokor, S. Cabrini, P. J. Schuck, M. C. Wu, and E. Yablonovitch, "Nanofocusing in a metal-insulator-metal gap plasmon waveguide with a three-dimensional linear taper," Nat. Photonics **6**, 838–844 (2012).
21. P. B. Johnson and R. W. Christy, "Optical constants of the noble metals," Phys. Rev. B **6**, 4370–4379 (1972).
22. E. D. Palik, ed., *Handbook of Optical Constants of Solids* (Academic, 1985).
23. R. F. Oulton, G. Bartal, D. F. P. Pile, and X. Zhang, "Confinement and propagation characteristics of subwavelength plasmonic modes," New J. Phys. **10**, 105018 (2008).
24. D. E. Chang, A. S. Sørensen, P. R. Hemmer, and M. D. Lukin, "Quantum optics with surface plasmons," Phys. Rev. Lett. **97**, 053002 (2006).
25. D. E. Chang, A. S. Sørensen, E. A. Demler, and M. D. Lukin, "A single-photon transistor using nanoscale surface plasmons," Nat. Phys. **3**, 807–812 (2007).